Spin-injection experiment

Mark Johnson and R. H. Silsbee
Laboratory of Atomic and Solid State Physics, Cornell University, Clark Hall, Ithaca, New York 14853-2501
(Received 22 June 1987)

The spin-injection experiment is a two-probe, spin-injector and detector experiment that has demonstrated the validity of a charge-spin coupling at a ferromagnet-paramagnet interface. The spin coupled signal is unambiguously identified by utilizing the Hanle effect; this approach results in a new, nonresonance technique for measuring conduction-electron spin-relaxation times in vanishingly small applied magnetic fields. Details of the spin-injection experiment are presented. The apparatus and techniques of sample preparation are described. Qualitative and quantitative analyses of the data are given, along with numerous examples. The results are discussed within the framework of the models developed in the preceding paper, and a few applications of the new technique are mentioned.

I. INTRODUCTION

In this paper we will give details of an experiment which demonstrates the validity of the concept of a coupling between charge and spin at the interface between a ferromagnetic and a paramagnetic metal. This experiment also demonstrates a new nonresonance technique to measure conduction electron spin-relaxation times in vanishingly small applied magnetic fields. The theory of the injection and detection technique is described in the preceding paper. Herein, we will first focus our attention on the experimental apparatus and the techniques of sample preparation. Then, qualitative and quantitative analysis of the data are given, and finally we discuss the results within the framework of the preceding paper (hereafter referred to as I).

Clean bulk aluminum provides a spin depth (the average distance an electron diffuses before losing its spin orientation) of order 100 μm at 4 K, and this length sets the scale of the experimental geometry. In order to avoid troublesome thermoelectric effects,[1] the drive current must be limited to tens of milliamps, and the contact resistances in the injector circuit should be as small as possible. It follows from this, and from the small value of the interfacial transport parameter η, that the observed signals are of order tens of picovolts, and a SQUID (superconducting quantum interference device) amplifier is used in the detector. The SQUID requires a low-input impedance source, and provides enough low-noise gain that the Johnson noise of the detector circuit is a significant limiting factor in the voltage resolution. These considerations necessitate minimizing the contact and wire resistances in the detector circuit. The sample geometry introduced in the preceding paper minimizes the background "mutual" resistance of the aluminum and consequently minimizes any magnetoresistance effects arising from Lorentz forces on charge flow. The requirements of the cryostat and electrical instrumentation are that they be capable of measuring a low source impedance with a resolution of a few picovolts in a magnetic field of order a hundred gauss, and in a temperature range of 2–60 K. All stray shunt conductances and reactances must be minimized.

The apparatus is described in the following section, sample preparation is presented in Sec. III, qualitative results in Sec. IV, quantitative results in Sec. V, the results are discussed in Sec. VI, and applications of the technique are given in Sec. VII.

II. APPARATUS

The detector was a SQUID sensor with picovoltmeter feedback electronics,[2] which was typically used with an ac bridge and a lockin at a frequency of 4 Hz.[3] Data have also been taken at strictly dc. Details of the operation of SQUID systems are described in the literature,[4] and we confine our discussion to the specifics of our circuit. A schematic is shown in Fig. 1. A current (of order tens of milliamps) is driven through the sample at contacts r_{c1} and r_{c2} inducing a voltage V_d (or current, depending on the feedback) in the detector circuit through contacts r_{c3} and r_{c4}. There are several independent contributions to the detector voltage: the spin coupled signal, a voltage from any remaining small mutual resistance (r_m) and stray reactance between injector and detector circuits,[5] and, at lower temperatures, a periodic magnetoresistance which will be discussed in another publication.[6] The bridge is used to null out these components to the detector voltage, in zero magnetic field.

The SQUID is used as a null detector for each of two feedback circuits, commonly called external feedback (EFB) and internal feedback (IFB). At dc in the EFB mode the switch S is closed and the feedback presents an impedance of 10 Ω to the sample circuit. This is much larger than any of the other resistances in the input circuit (the contact resistances r_{ci} are the next largest, of order of 10 mΩ), and the result is an open circuit voltage measurement. The measured voltage $V_{0,\mathrm{EFB}}$ is given by[4,5]

$$V_{0,\mathrm{EFB}}=\frac{V_d R_{F,\mathrm{EFB}}}{r_{std}}=10^8\ V_d\ \mathrm{V}\ , \tag{1}$$

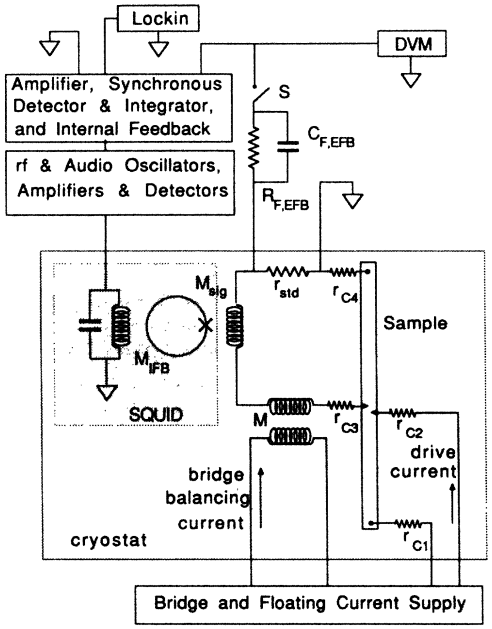

FIG. 1. Schematic diagram of the detector circuit, including the SQUID, the feedback electronics, and the bridge.

where $R_{F,\mathrm{EFB}}$ is the feedback resistor, and V_d is the true voltage from detector to the end of the sample (we usually refer to V_d as the magnetic field dependent voltage of interest; in the ac measurements the zero field baseline voltage contribution from r_m has typically been nulled out). The gain in the EFB mode is frequency dependent, and begins to roll off at just a few Hz.

The IFB mode measures the current (of order nanoamps) in the detector circuit when the impedance of the circuit is small. Let Z_{det} be the total impedance of the detector circuit (of order 10 mΩ, 10 nH), M_{sig} the mutual inductance from detector circuit inductor to SQUID, M_{IFB} the mutual inductance from the tank circuit to the SQUID, and $R_{F,\mathrm{IFB}}$ the IFB feedback resistor. Then the measured voltage $V_{0,\mathrm{IFB}}$ at dc is

$$V_{0,\mathrm{IFB}}=\frac{V_d M_{\mathrm{sig}} R_{F,\mathrm{IFB}}}{Z_{\mathrm{det}} M_{\mathrm{IFB}}} \ . \tag{2}$$

Internal feedback has a much better frequency response; in our mode of operation, it rolls off at about 1 kHz. The ratio of the two voltages depends on the flux-voltage characteristic of the particular SQUID, but is typically given by

$$\frac{V_{0,\mathrm{EFB}}}{V_{0,\mathrm{IFB}}}=\frac{Z_{\mathrm{det}} R_{F,\mathrm{EFB}} M_{\mathrm{IFB}}}{r_{std} R_{F,\mathrm{IFB}} M_{\mathrm{sig}}}=500\ Z_{\mathrm{det}} \ . \tag{3}$$

In an experiment, the voltages $V_{0,\mathrm{EFB}}(I)$ and $V_{0,\mathrm{IFB}}(I)$ are measured as functions of current at dc and compared to determine Z_{det}. This calibrates IFB for voltage measurements at frequencies above dc. The experiment is typically performed ac so that we can use a bridge to null out background signals and a lockin to filter out noise. The IFB mode is used because of its superior frequency response. A secondary function of the bridge is to provide a means to cross check the calibration of our system.[5] We have also taken data at dc to verify that stray reactances are not giving us spurious signals. Notice that the current in the detector circuit is a small (10^{-6}) fraction of the injected current making the experiment vulnerable to stray shunt impedances between injector and detector circuits.

Typically, the only filters used were the time constants of the lockin. The calculated Johnson noise of the detecting circuit is

$$V_{jn}=7.4\times10^{-12}\sqrt{Z_{\mathrm{det}}T}\ /\sqrt{Hz} \ . \tag{4}$$

For a representative value of the detector loop impedance, and for a noise bandwidth of 0.3 Hz, the predicted noise is about 1 pV. The noise in the data of Fig. 2 is about twice this value. More typically, noise is 5–10 pV.

It is interesting, as well, to calculate the sensitivity of the apparatus in terms of spin parameters. Recall from I that we calculated the number of nonequilibrium spins Δn that correspond to a measured voltage V_d. The free-electron density of states near E_F for a single spin subband[7] is $N_{\mathrm{up}}(E_F)=3n/4E_F$. Then we have

$$\Delta n=2\int_{E_{F;p}}^{E_{F;p}+eV_d} N_{\mathrm{up}}(E)dE \ ,$$

which gives

$$\Delta n=\frac{3neV_d}{2E_F} \ ,$$

or, for a detector measuring with efficiency η,

$$\frac{\Delta n}{n}=\frac{3eV_d}{2\eta E_F} \ . \tag{5}$$

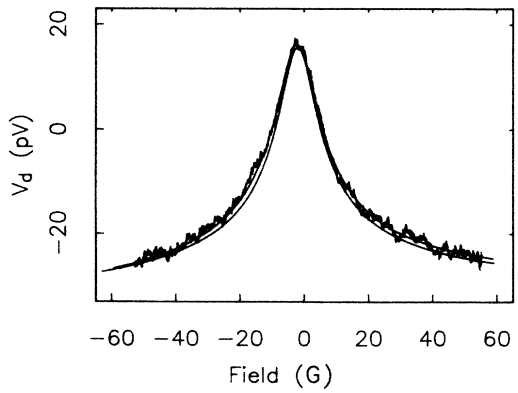

FIG. 2. Sample Walrus 7-50. $T=4.3$ K, $L=50\,\mu\mathrm{m}<\delta_s=450$ μm, $I=22$ mA, $T_2=9\times10^{-9}$ s, $\eta=0.067$, $\alpha=0°$ ($\xi=1.0$), the background slope is 2%, the sweep is along $\hat{\mathbf{x}}$, and D is independently determined to be $D=1.1\times10^5$ cm^2/s. In TESR this is the thin limit. This is an example of an absorptive Hanle signal. Note that the noise is a few picovolts. This is typical noise when everything happens to work exactly right. The second fit is for $T_2=1\times10^{-8}$ s, and is noticeably too narrow. Note that here the zero point on the abscissa has been arbitrarily chosen by the bridge.

For a sensitivity of 3 pV in aluminum ($E_F = 12$ V) and for $\eta = 0.07$, one finds $\Delta n/n \approx 5 \times 10^{-12}$. Consider what this means: if there are 2×10^{11} spins in equilibrium, 10^{11} up and 10^{11} down, and *one* of the down spins is flipped up, it would be detected. This bodacious sensitivity suggests speculation about using the technique to probe single spin events. Using refined sample preparation techniques, such as molecular beam epitaxy (MBE), and sophisticated photolithography or *e*-beam lithography, it is quite possible to make a sample that contains the order of 10^{11} conduction electrons, $\sim(1\ \mu\text{m})^3$ of metal or $\sim(1-10\ \mu\text{m})^3$ of semiconductor. This, and other applications, will be discussed in Sec. VII.

The equivalent magnetic field that would cause an equilibrium magnetization of this magnitude can also be calculated:

$$H = \frac{M}{\chi} = \beta \frac{\Delta n}{\chi} , \tag{6}$$

where χ is the free-electron Pauli susceptibility:

$$\chi = \beta^2 \frac{m k_F}{\hbar^2 \pi^2} ,$$

β is the Bohr magneton, m the electron mass, and k_F the Fermi wave vector. Using $n \approx 10^{23}$ electrons per cc for aluminum, one finds $H \approx 6$ mG. Note that in an experiment, this magnetization must be established as a departure from equilibrium in order to be detected by our technique.

The cryostat and dewar hang between the pole faces of a conventional magnet that can be rotated through 360°, and all three (together) are floated off the floor by a truck tire inner tube to decouple them from building vibration. The field is controlled by a linear sweep circuit. In a typical experiment, V_d is digitized and stored in a Nicolet storage oscilloscope as the field is swept. The data are then stored on floppy disks, and later transferred to a computer for analysis.

III. SAMPLE PREPARATION

The paramagnetic material in this experiment was pure aluminum with a bulk residual resistivity ratio (RRR) at 4 K of 10^4 before processing. It was cold rolled, annealed, and sliced into a bar 50 μm × 100 μm × 1.5 cm. This was fixed (with a thin layer of epoxy) to a sapphire substrate, and coated with a 1 μm layer of polyimide. An array of windows, 15 μm × 45 μm, was photolithographically defined and chemically etched through this insulating layer to expose the surface of the aluminum. The samples were respun with photoresist, and a pattern of 50 μm × 50 μm squares was exposed and developed. Each square overlapped a window (Fig. 3). The samples were placed in a vacuum system with a base pressure of about 10^{-7} Torr. They were ion milled, to clean the aluminum surface, and a 650 Å film of 70% nickel, 30% iron (initial composition), permalloy was *e*-beam evaporated, followed by 2300 Å of gold for passivation. The photoresist was then lifted off, leaving an array of gold covered permalloy squares above the sample surface. The polyimide was pinhole free, allowing us to define a small region of interfacial contact to the aluminum while having a relatively large pad with which to make wire connections. The profile of the etched polyimide was gradual enough to ensure a continuous film. A control sample was made by an identical procedure, except that no permalloy was deposited.

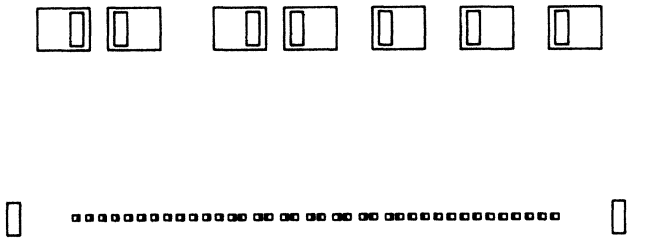

FIG. 3. The photolithographic patterns used in sample preparation. Bottom: the array of windows and pads are photolithographically defined on a 100 μm wide bulk metal sample. Top: close-up of the patterns. The windows, 15 μm × 45 μm, are etched to expose the surface of the metal sample. The larger squares, 50 μm × 50 μm, are metal films that sit on the insulating polyimide and overlap the windows to the metal surface. Indium wires are connected to these squares. The windows are spaced in multiples of 50 μm, center to center.

Indium wires, of about 30 μm diameter at the tip (freshly drawn from a melt), were cold welded to the junctions and led to the injecting and detecting circuits, whose resistance is of order 10 $m\Omega$. The resistance of the permalloy-aluminum junctions is estimated to be less than a few milliohms, but we do not believe them to be clean, metal to metal interfaces. A tunneling conductance measurement, at 1 K, of a similarly prepared junction showed that it was *not* a good tunnel junction. The samples had a residual resistivity ratio (RRR) of about 1100 after processing; the mean free path (35 μm) is probably dominated by surface scattering.

The magnetization of ideal thin ferromagnetic films on an ideal surface remains nearly in the plane of the films for applied fields of any orientation and magnitude small compared to the $4\pi M$ of the film. At low temperatures, application of an external field in the plane of the film can convert an inhomogeneous magnetic structure into a single domain film. The orientation of the domain is determined by a combination of the applied field and any of several anisotropies.[8] For example, the geometric aspect ratio of the film, small fields present during deposition, strains in the film, or interactions with the substrate that prefer a crystallographic orientation can cause anisotropy forces that may determine the orientation of the domain. These forces can be characterized by a field B_0 required to reverse or reorient the magnetization. For permalloy films of high quality on sapphire substrates, these fields are typically on the order of a few gauss or less.

The films used in our experiment show substantial in-plane anisotropy of unknown origin. Once established in a particular direction by application of a large applied field along an axis, the magnetization appears to be stable

against reversal up to an opposing field (along the opposite axis) B_0 of about 100 G. No two films have the same anisotropies, and the value of B_0 varies for different films by an amount of order 10 G. It is stable against large in-plane rotation for applied fields in the $\hat{x}$ direction of less than 50 G. The geometry of the experiment is depicted in Fig. 4 of I, and discussed at great length therein. In a typical experiment, a field of a few hundred gauss is applied along $-\hat{z}$ to define the magnetization of polarizer and analyzer to be parallel to each other (we "soak" the films in a field). B_z is then reduced to zero and the field is swept along $\hat{y}$, or at angle ϕ from $\hat{z}$ in the $\hat{y}$-$\hat{z}$ plane. The component of field along $\hat{z}$ is always less than B_0, so that the initial alignment of injector and detector is preserved. The sweep rate is of the order of a gauss per second, which maintains SQUID stability and matches the rate at which we can digitize the data for the bandwidth we use. The field in the $\hat{y}$-$\hat{z}$ plane is provided by a conventional magnet. Field sweeps of a narrower range have also been performed along $\hat{x}$, using a solenoid wrapped around the dewar.

Figure 4 is a scanning electron micrograph (SEM) of a portion of an unused window and square on the control sample. The surface of the square pad, which sits on the polyimide, is smooth. The window is lower than the pad (by the thickness of the polyimide, about 1 μm) and the surface of the aluminum (here covered by 2600 Å of gold) revealed through the window is pitted. Examination by SEM reveals that the profile of the window edge (determined by the etching of the polyimide) ranges from near vertical to approximately a 60° slope for different windows, and that all of the examined windows had pitted surfaces (of varying degree). The scale of pitting is a few thousand angstroms. We believe that the surface of the aluminum, after cold rolling, is lightly scratched and pockmarked, and that the chemical processing (which involves a sodium hydroxide based photoresist developer) exacerbates the surface abnormalities, resulting in deeper pits. It is possible that the roughness of the surface impedes domain wall motion, thus requiring larger fields to move the domain walls and therefore contributing to the large value of B_0.

FIG. 4. SEM of window and pad from the control sample, Walrus 8. The light area is a 2600 Å gold film, the dark is polyimide with*out* metalization over the bulk aluminum bar sample. The window has been etched through the polyimide to the surface of the aluminum. Note that the surface is pitted. The film of the pad lies on top of the insulating polyimide, which is a micron thick. Note that the film of the pad has a smooth surface. The film is continuous and overlaps the window, making interfacial contact with the aluminum over the area of the window. At lower left, part of the pad has been torn off during "liftoff."

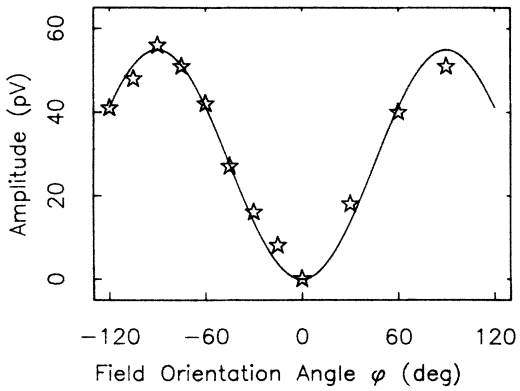

FIG. 5. The symbols give the Hanle signal amplitude as a function of field orientation angle ϕ. The line is the curve $\sin^2\phi$.

The $4\pi M$ of our permalloy was determined from ferromagnetic resonance (FMR) measurements to be about 10 kG. Our films have a large aspect ratio ($\approx$45 μm/650 Å), which ensure that the fields are contained almost entirely within the film. One can show that the fringe fields from uniform thin ferromagnetic films are only a few gauss at positions as close as a few microns, except at the ends of the films, where statistically the electrons spend little time. However, the permalloy may not be continuous across the window edge, and the interfacial film may experience locally strong fields at the discontinuity. Furthermore, since it is apparent that the surface of the aluminum is quite rugged on a scale of thousands of angstroms, although the average film magnetization is in the plane of the window (the $\hat{x}$-$\hat{z}$ plane), there may well be large local deviations of the magnetization. These inhomogeneities fall off exponentially with distance from the surface and on average the electrons spend little time in the inhomogeneous region, and are further able to average over the inhomogeneities that are experienced.

IV. QUALITATIVE RESULTS

In I we have presented the theory of spin injection and detection, and noted a number of characteristics of the expected signal. In the following section we present the results of quantitative fits to the observed Hanle signal, the destruction of the spin coupled signal with application of a magnetic field. This section summarizes other features of the results which suggest the spin coupling to be the source of the observed signals. All of the expected characteristics have been observed and verified in the four samples with which data were taken. Identically performed sweeps on a control sample showed no Hanle signal. A broader magnetic signal (a few hundred gauss

wide) was observed at lower temperatures in both the ferromagnetic and control samples, and will be discussed in another publication.[6] We were also able, under certain conditions, to manipulate the magnetization of individual films (injector or detector), thus changing the relative angle between injector and detector, and then to observe the predicted change in character of the signal as discussed in the preceding paper.

The Hanle effect, the destruction of the signal by an applied magnetic field, is effective only on that portion of the magnetization which is perpendicular to the applied field. It was predicted that the signal amplitude as a function of orientation ϕ (refer to Fig. 4 of I) of applied magnetic field should vary as $\sin^2\phi$. Figure 5 compares that prediction with data from the sample Walrus 7-50 at constant temperature.

The sign of the spin coupled signal and its variation with applied field depend upon the relative orientations of the magnetizations in the two ferromagnetic films, being positive if the magnetizations are parallel, negative if antiparallel. In Fig. 6 is a demonstration of an experiment in which we manipulate the orientations of the magnetizations of the films. The magnetization of both films is first established along $-\hat{z}$ (parallel) by application of a large field, and then the field is swept from negative to positive. Note that, as predicted, there is no Hanle signal near $B=0$. There is, however, a dramatic change in signal at $B_{0,1}$, with recovery to the original signal at $B_{0,2}$. Recall that the value of B_0 varies by several gauss for different films. At $B_{0,1}$ the injector (or detector) magnetization has reoriented by 180° and now points along $+\hat{z}$. The films are now antiparallel, and there results a reversal of sign of the spin coupled signal. At $B_{0,2}$ the detector (or injector) has flipped its orientation as well. Now both films are aligned (parallel) along $+\hat{z}$ and the original signal is recovered. Further confirmation of this interpretation is evidenced in Fig. 7. Here we have halted a $\hat{z}$ sweep between $B_{0,1}$ and $B_{0,2}$, reducing the field to zero, and then swept the field along $\hat{y}$. The Hanle signal is observed, but with opposite sign, a dip rather than a peak.

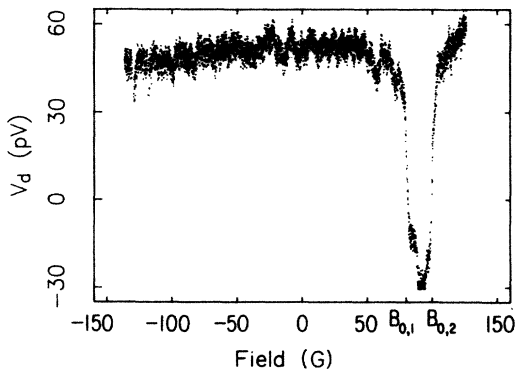

FIG. 6. Typical $\hat{z}$ sweep for sample Walrus 7-50, from negative to positive fields. At $B_{0,1}$ the injector (or detector) magnetization has reoriented by 180° and now points along $+\hat{z}$, resulting in a reversal of sign of the spin coupled signal. At $B_{0,2}$ the detector (or injector) has also flipped its orientation to be along $+\hat{z}$, and the original signal is recovered. Note that the "dip" does not fully reach −45 pV; this simply means that there is not quite complete reversal of one film before the direction of the magnetization begins to change in the second.

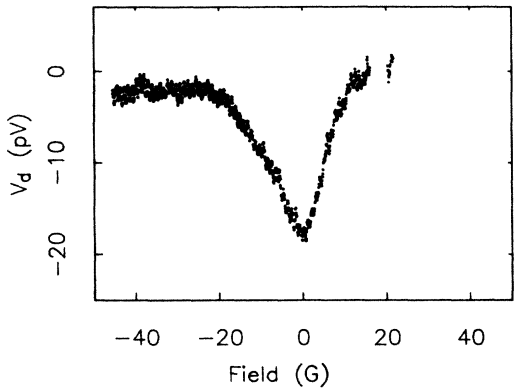

FIG. 7. A $\hat{z}$ sweep is halted between $B_{0,1}$ and $B_{0,2}$ (refer to Fig. 6). The injector and detector now point in opposite directions. The field along $\hat{z}$ is reduced to zero, and a field sweep along $\hat{y}$ is performed. The resulting Hanle signal now appears with opposite sign, as expected for a detector antialigned with the injector.

When the magnetizations of the films are aligned, the appearance of the Hanle signal for field sweeps perpendicular to the orientation of the injected spins should be "absorptive," i.e., a bell-shaped curve. If the magnetizations are perpendicular to each other, the appearance of the signal should be "dispersive," changing signs at $B=0$ and diminishing in amplitude for increasing field magnitude. For arbitrary orientation, the shape of the Hanle signal is predicted to be a mixture of absorptive and dispersive characters. The degree of admixture depends upon the orientations of the magnetizations relative to each other and relative to the applied field.

Field sweeps along $\hat{x}$ and $\hat{y}$ typically show a signal which is a mixture of the predicted absorptive and dispersive shapes, with a reasonable width and amplitude. In principle, the angle α between the magnetizations in the two films can be deduced from the degree of admixture of the dispersive signal; in practice there were no simple systematics, a consequence, we feel, of the surface pitting or facetting noted in Fig. 4. For the nonplanar surface, the local magnetization at the interface will not be parallel to the average interface orientation, and with appropriate facetting patterns a wide variety of values for α could be imagined. For example, one sample (Walrus 6-300) showed an absorptive signal for B along $\hat{y}$, an absorptive signal of diminished amplitude for B along $\hat{z}$, and a purely dispersive signal along $\hat{x}$. The existence of a signal for field sweeps along $\hat{z}$ is a departure from the expected characteristics, previously described, of the signal for ideal, well-behaved ferromagnetic films. However, the existence of the $\hat{z}$-sweep signal can be understood in the context of a facetted interface. A simple explanation can be given by imagining the surface to be like a washboard, whose corrugations are parallel to $\hat{x}$. Then some component of the injected magnetization will be perpendicular to $\hat{z}$, will be destroyed by the Hanle effect when

$\gamma BT_2 > 1$, and a Hanle signal will appear for this orientation of field sweep.

V. QUANTITATIVE RESULTS

As a detailed test of the theory and interpretation, data were taken on four sets of probes of different separations (two sets on each of two samples), over the temperature range 4–55 K, and fit to Eq. (24) of the preceding paper. Examples of data and fits are shown in Figs. 2 and 8–10 (typically the zero point on the abscissa has been arbitrarily determined by the bridge). In these fits, the only free fitting parameters, each with a clear, physical interpretation, were the efficiency of interfacial magnetization transport η, the conduction-electron spin-relaxation time T_2, a dispersive and/or absorptive admixture parameter α, which is the relative angle between injector and detector films, and a small, linear baseline correction (to a drift of unknown origin). The relevant electrical and geometric factors were determined directly. The diffusion constant as a function of temperature, $D(T)$, was determined in the following way. The injector and detector probes, separated by distance L, were crossed on a control sample of cross-section area A (the right probe was grounded at the left end of the bar, and vice versa). There was then a large voltage V_d at the detector given by

$$V_d = \frac{\rho(T)L}{A} I \ .$$

From this, the resistivity as a function of temperature $\rho(T)$ was measured, and $D(T)$ was calculated from an Einstein relation[9]

$$D(T) = \frac{(1+b_0)[\rho(T)]^{-1}}{e^2 N^*(E_F)} \ ,$$

where $(1+b_0)^{-1}$ is the exchange enhancement of the susceptibility and $N^*(E_F)$ is the density of states at the Fermi surface, determined by a specific-heat measurement.[10]

A critical parameter in discussing the data is the spin depth $\delta_s = \sqrt{2DT_2}$. This is the average distance a spin diffuses before losing its orientation in a scattering event. Figure 2 presents data from an $\hat{x}$ sweep of a sample where $L = 50\ \mu\text{m} \ll \delta_s = 450\ \mu\text{m}$. In transmission electron-spin resonance (TESR), $L \ll \delta_s$ is known as the "thin" limit. The average precessional phase accumulated by a spin, in field $B = (\gamma T_2)^{-1}$, in the time it takes to diffuse from the injector to the detector, is small. Because the diffusion time L^2/D is short compared with T_2, the feature width is characterized by T_2, and the probe separation plays no important role in determining the line shape. The line

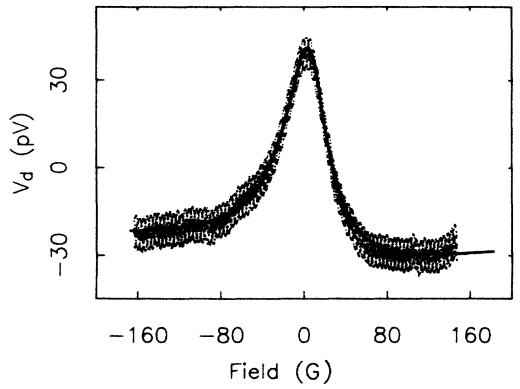

FIG. 8. Sample Walrus 7-50. $T = 45$ K, $L = 50\ \mu\text{m} < \delta_s = 90\ \mu\text{m}$, $I = 34$ mA, $T_2 = 3\times10^{-9}$ s, $D = 1.34\times10^4$ from the independent resistivity measurement. Here $\alpha = 19°$. The increased linewidth for increasing temperature is apparent by comparison with Fig. 2.

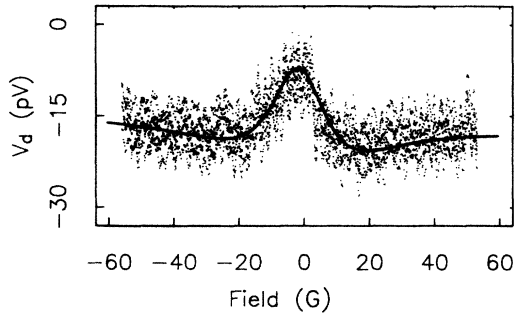

FIG. 9. Sample Walrus 6-300. $T = 36.6$ K, $L = 300\ \mu\text{m} > \delta_s = 170\ \mu\text{m}$, $I = 47$ mA, $T_2 = 5\times10^{-9}$ s, $\eta = 0.051$, $\alpha = 12°$, the background slope is 2%, and D is independently determined to be $D = 2.9\times10^4$ cm^2/s. This is the average of three sweeps at $\phi = 5°$ from $\hat{y}$. In TESR this is known as the thick limit; note the development of wings beyond the minima.

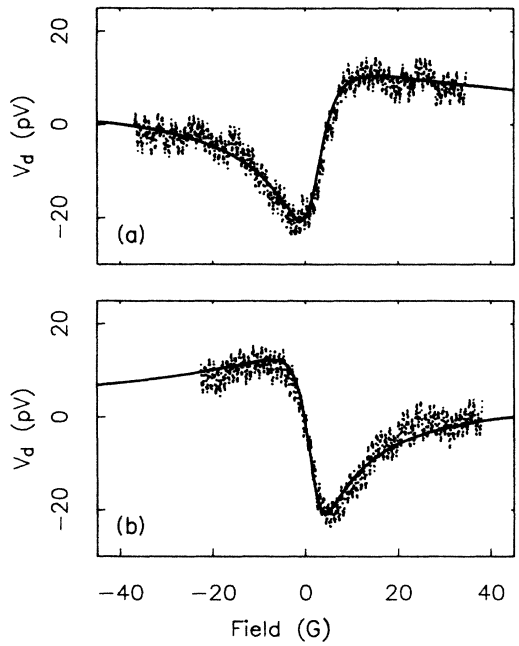

FIG. 10. Sample Walrus 7-200. The magnetization in the films of this sample has a peculiar orientation. (a) The films are soaked in a field of several hundred gauss in the $+\hat{y}$ direction, and the field is swept from positive to negative with the result $\alpha = 124°$. (b) The films are soaked in a field along $-\hat{y}$, and the field is swept from negative to positive with the result $\alpha = -124°$.

through the data is a fit from Eq. (24) of I, using the parameters $T_2=9\times10^{-9}$ s, $\eta=0.067$, and D was determined from the resistivity to be $D=1.1\times10^5$ cm^2/s. For this fit we have used $\alpha=0°$; that is to say it is purely absorptive in character. In general, the baseline of our data has a slight slope, of the order of a few percent, of unknown origin. Here, a linear term allowing for a 2% baseline slope has been added. The second line is a solution to Eq. (24) of I using $T_2=1\times10^{-8}$ s. It is noticeably too narrow for the data, and the clear discrepancy indicates the sensitivity of the model to variation of a fitting parameter. In Fig. 8 are plotted data from a $\hat{y}$ sweep of the same sample at $T=45$ K. Here $L=50$ μm $<\delta_s=90$ μm so we are still in the thin limit, and $\alpha=19°$. The increase in linewidth with increasing temperature is clearly shown by comparison with Fig. 2.

Figure 9 presents data from a $\hat{y}$ sweep of a sample with $T=36.6$ K, $L=300$ μm $>\delta_s=170$ μm. In TESR this is known as the "thick" limit. In this regime, the diffusive speed is slower, L is longer, and it takes a longer time for the spins to reach the detector. In contrast with the thin limit, the diffusion time between injector and detector is long compared with T_2. During the mean diffusion time, the electrons will have accumulated substantial phase which will give rise to a signal reversal as seen in Fig. 9. The detailed shape of the feature is now characterized by both T_2 and the time associated with the diffusion of the magnetization from $x=0$ to $x=L$. The plot shown is the average of three data sets.

In Fig. 10 we illustrate an attempt to modify the orientation of the magnetization of the injector and detector films, in order to investigate the nature of the unknown anisotropy forces. This figure presents data from $\hat{y}$ sweeps of sample Walrus 7-200 at 4.3 K. For this sample, the signal was predominately dispersive with a negative absorptive component for all sweep orientations ϕ, which suggests that the angle between injector and detector is near perpendicular, but there is always a substantial antialigned component. In Fig. 10(a), the sample is soaked in a field of several hundred gauss along $\hat{y}$, and the field is swept from positive to negative with the result that, according to the fit, $\alpha=124°$. In Fig. 10(b), the sample is soaked in a field of a few hundred gauss along $-\hat{y}$, and the field is swept from negative to positive. Now the result is $\alpha=-124°$; the dispersive component has changed signs while the (negative, antialigned) absorptive part is unchanged. A possible explanation for this behavior is that the magnetization of these films is oriented, by unknown forces, primarily along the $\hat{x}$ axis, one along the $\hat{x}$ direction and the other along the $-\hat{x}$, and that each has a component along the $\hat{z}$ direction. The latter component is presumably reversed completely by soaking, while the former component is completely unaffected.

The validity of the interpretation of the full collection of data in terms of the spin coupling model may be tested by comparing the value of the coupling efficiency η determined from different data sets. These values, from the fits of 17 data sets, over a temperature range of 4–45 K, with probe separations of 50, 200, and 300 μm (data from $L=100$ μm have yet to be quantitatively analyzed), and for sweeps along $\hat{x}$ and $\hat{y}$ varied within $\pm25\%$ of a mean value of 0.061, and are listed in Table I. Consistency among the data sets for a given pair of probes was about $\pm10\%$. Most importantly, there was no systematic variation in η with temperature, even though the range in observed signal amplitude varied by as much as seven to one (0.25 nΩ–1.8 nΩ). The fact that a single set of fitting parameters consistently describe a signal that varies in amplitude by an order of magnitude gives us confidence in the validity of our one-dimensional model. The variation in η for each pair of probes is mostly caused by variation in calibration of the IFB. From day to day and run to run the measured value of $Z_{\rm det}$ varied about 15% (recall that η scales with the square root of voltage). $Z_{\rm det}(T)$ was measured on a control sample and normalized according to its value at 4 K. Typically, for a given sample and run, $Z_{\rm det}(T)$ was calculated from its particular value at 4 K and the temperature dependence of the control.[11]

TABLE I. Consistency of η for varying conditions L, T, and α. Changes in α were achieved by different soaking of the films, and varying the orientation ϕ of the applied field, as discussed in the text.

L (μm)	T (K)	α (deg)	η
50	4.3	0	0.067
50	21	−23	0.075
50	27	−19	0.072
50	27	−23	0.072
50	27	6	0.070
50	34	19	0.068
50	45	19	0.066
200	4.3	124	0.043
200	4.3	−124	0.043
300	4.3	10	0.056
300	4.3	10	0.057
300	9.5	−23	0.054
300	9.5	−6	0.049
300	9.5	19	0.046
300	18	−19	0.056
300	29	14	0.046
300	37	12	0.051

As a final test of the theory, the values of T_2 extracted from the fits are compared with values of T_2 determined by a conventional TESR method. Because of the g anisotropy of aluminum,[12] the comparison should be made with measurement performed at the lowest frequency possible. Lubzens[13] has measured the relaxation time of conduction electrons in aluminum at 1.3 GHz, a low enough frequency that the g anisotropy should result in little broadening, and in Fig. 11 the comparison is made. One expects contributions to linewidths from spin-flip scattering with surfaces, impurities, and phonons. At low temperatures the former two processes dominate. This residual width is expected to differ for samples of different purity and geometry. In Fig. 11 we subtract this residual width to isolate the temperature dependence of T_2, i.e., the phonon contribution $T_{2,\rm ph}$, and note that they compare well.

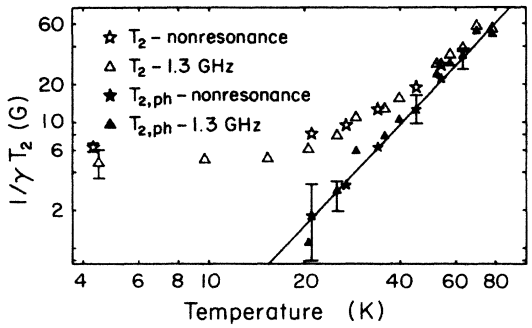

FIG. 11. Comparison of relaxation times as measured by the new, nonresonance method, and TESR at 1.3 GHz. For the solid symbols, the residual widths have been subtracted to isolate the temperature dependence of T_2.

VI. DISCUSSION

In the Appendix of Ref. 1 is a rigorous calculation of the magnetic current that flows across a ferromagnet-paramagnet interface. There are two regimes of interest, identified by comparison of the interface conductance G to the spin conductance g_i of the ferromagnet and paramagnet. We define $g_i=(\sigma_i/\delta_i)A_i$ as the ratio of the bulk conductivity to spin depth multiplied by an area relevant to spin diffusion; it is the conductance of a length of the bulk material equal to one spin depth. In the limit $G \ll g_f, g_p$, the spin distributions are little disturbed on either side of the interface as a consequence of magnetization transport across the interface and it is the interfacial transport parameter η which entirely determines the ratio of magnetic to electric current. In the other limit, $G \gg g_f, g_p$, the magnetization current is determined by a parameter p which, analogous to η, describes the spin subband asymmetry *within* the ferromagnet, $p=[(J_{\text{up}}-J_{\text{down}})/J]_f$. In this limit, essentially all the magnetization current from the ferromagnet is carried into the paramagnet, if there is high diffusion and rapid relaxation in the paramagnet. Low diffusion and long relaxation in the paramagnet that lead to substantial build up of δM near the interface will impede and diminish the magnetization current, a second-order effect.

In our experiment, g_p is measured to be (using the cross-sectional area of the bar for A_p) of order 10^6 mho. Although it is somewhat more difficult to determine g_f (in particular δ_f is uncertain), a reasonable approximation is of the order 10^5 mho. Estimating our interfacial conductance to be about 10^3 mho, we believe that we are in the regime $G \ll g_f, g_p$, and that we can analyze our results in terms of interfacial transport parameter η.

Our values of η are significantly less than Tedrow *et al.* have measured.[14] For a permalloy composition of 70% nickel and 30% iron, they reported 40% spin current polarization ($\eta=0.40$). There are several possible explanations[15] for our observation of a smaller η. The first is that our permalloy films may not be continuous over the coarse surface of the aluminum. In this event, the magnetic current would be diluted by nonpolarized current passing from the gold directly to the aluminum. We discount this possibility for two reasons. The permalloy film was evaporated at normal incidence to the surface, and its thickness of 650 Å should be enough to guarantee continuous coverage. Furthermore, the value of η is *not* dramatically different between sample Walrus 7-50, which must have a fairly smooth surface (the signal is mostly absorptive for $\hat{\mathbf{x}}$ and $\hat{\mathbf{y}}$ sweeps, and is zero for $\hat{\mathbf{z}}$ sweeps) and presumably continuous coverage, and the other samples, which behave in a manner consistent with pitted or facetted surfaces (a relatively large dispersive component for some sweep orientation).

The second possibility is that the composition of our permalloy changed during the process of evaporation. It is difficult to analyze the stoichiometry of our films because they are thin, because there is a thick gold film covering them, and because nickel and iron have similar atomic number. We know, however, that the measured $4\pi M$ of 10 kG is approximately correct for 70-30 permalloy.

A third plausible explanation is that the films are not aligning as single domains. We do not believe this to be an important factor for the following reason. In Fig. 6 the data show a sharp transition from positive to negative signal, and back to positive again. This suggests that the films of sample Walrus 7-50 are acting as single domains. The same kind of data [wherein the films were soaked in a field $B > B_0(-\hat{\mathbf{z}})$, then the field was swept along $\hat{\mathbf{z}}$, through zero and past $B_0\hat{\mathbf{z}}$] have been taken for several samples. In sample Walrus 6-300, there is a smooth transition from positive to negative voltage, and back again, which is more gradual, taking place over a field range of about 250 G (to be contrasted with the range of 20 G in Fig. 6). This suggests that these films are not flipping as single domains. However, the average values of η for sample Walrus 7-50 ($\eta=0.070$) and Walrus 6-300 ($\eta=0.052$) are not dramatically different. We therefore believe that deviations from uniform magnetization (perhaps caused by the rugged surface) in the film could account for variations in η of tens of percent, but not factors of 5 or 7, which is the discrepancy between our results and those of Tedrow *et al.* The reproducibility of η for all our different samples further supports this conclusion.

We consider a fourth possibility to be the more likely explanation for the discrepancy: the two techniques involve different transport processes. The interfaces in the samples of Tedrow *et al.* were good tunnel junctions, and tunneling was the transport process in their experiment. We believe that our contacts are neither good tunnel junctions nor clean metal-metal interfaces. Rather, it is likely that there is a thin, uneven layer of aluminum oxide between the permalloy and aluminum, and that there are pinhole current leaks (of unknown diameter) through this insulating oxide. If the pinhole has a diameter that is large compared to an electronic mean free path, it is said to be in the Maxwell limit and the interfacial resistance is dominated by the spreading resistance in the metals. If the pinhole has a diameter small relative to an electronic mean free path, it is said to be in the Sharvin (or Knudsen) limit, and the conductance for each band b is determined by the size of the pinhole, the density of states at

the Fermi surface, the Fermi velocity, and the electron transmission probability $\langle t_b \rangle$.

In I we developed an expression for the interfacial conductance per unit area $g_{b,s}$ from band b and subband s of one metal to a contiguous free-electron metal. This conductance depends on the band structure of the metal, and on the nature of the transport process. The interfacial magnetization transport parameter η was defined in terms of sums and differences of $g_{b,s}$, and is therefore expected to vary for different kinds of transport. Consider a simple, two-band model for a transition-metal ferromagnet, a reasonable picture of permalloy. There are two bands at the Fermi surface. The 4s band is free-electron like, and has very little or no subband imbalance. The 3d band has a substantial subband imbalance, and the electrons are less itinerant, have smaller Fermi velocity, and have greater effective mass. Due to the subband imbalance, the density of states near the Fermi surface (relevant for those electrons contributing to the conduction) is inequivalent for the two subbands, and as a result, current from this band is polarized.

From I we write the following expression for η for a two-band ferromagnet:

$$\eta=\frac{(g_{3d,\mathrm{up}}-g_{3d,\mathrm{down}})+(g_{4s,\mathrm{up}}-g_{4s,\mathrm{down}})}{g_{3d,\mathrm{up}}+g_{3d,\mathrm{down}}+g_{4s,\mathrm{up}}+g_{4s,\mathrm{down}}},$$

where

$$g_{b,s}=e^2[N(E_F)\langle v_\perp\rangle\langle t\rangle]_{b,s}\ . \tag{7}$$

In these expressions, $\langle v_\perp \rangle$ is an angular average of the perpendicular component of the Fermi velocity, and $\langle t \rangle$ is an angular average of an interfacial transmission coefficient, which depends on the transport mechanism. To illustrate how η might vary, note that $(g_{4s,\mathrm{up}}-g_{4s,\mathrm{down}})\approx 0$, and consider first a process for which $g_{3d} \gg g_{4s}$; then $\eta_1 \approx (g_{3d,\mathrm{up}}-g_{3d,\mathrm{down}})/(g_{3d,\mathrm{up}}+g_{3d,\mathrm{down}})$. Compare this with a process wherein $g_{3d} \ll g_{4s}$. Even if the relative difference in subband conductance, $(g_{3d,\mathrm{up}}-g_{3d,\mathrm{down}})/(g_{3d,\mathrm{up}}+g_{3d,\mathrm{down}})$, is unchanged, the magnetization transport parameter for the latter process, η_2, will be reduced from that for the first by the ratio $g_{3d}/(g_{3d}+g_{4s}) \ll 1$.

The ratio of interfacial conductance for bands 3d and 4s is, from Eq. (7),

$$\frac{g_s}{g_d}=\frac{N_s(E_F)}{N_d(E_F)}\frac{\langle v_s\rangle}{\langle v_d\rangle}\frac{\langle t_s\rangle}{\langle t_d\rangle}\ . \tag{8}$$

In the simple case that $\langle v_b \rangle = (\mathrm{const}) v_{F;b}$ the ratio simply reduces to $g_s/g_d = \langle t_s \rangle / \langle t_d \rangle$. For a Sharvin pinhole, in the simplest picture, $\langle t \rangle$ is just the geometric ratio of the pinhole area to that of the interface, $\langle t_d \rangle = \langle t_s \rangle$, and $g_s/g_d \approx 1$ (the contributions to the interfacial current from each band are comparable). For a Maxwell pinhole, however, one can show that,[5] with the assumption of comparable scattering rates for s and d band electrons,[16,17] the ratio of interfacial conductance for the s and d bands is given by

$$\frac{g_s}{g_d}=\frac{N_d(E_F)}{N_s(E_F)}\ . \tag{9}$$

For nickel, the ratio $N_d(E_F)/N_s(E_F)$ is of the order of 10 to 1. This result predicts that the weakly polarized s band will dominate interfacial conductance, and the magnetic current will be diluted as a result. For a tunneling calculation, the exact form of g will depend on the particular shape of the barrier and other assumptions. It can be shown that a reasonable expectation is $g_s/g_d \leq 1$. We thus conclude that a probable explanation for the fact that the measured value of η is less in our experiment than that of Meservey *et al.* is that our interfacial current contains a relatively larger component of unpolarized electrons (from the 4s band), and the magnetization current through our interfaces is diluted relative to that of Meservey *et al.*'s tunnel junctions.

VII. APPLICATIONS AND CONCLUSIONS

In this final section we will list some of the unique features of the method that make it a useful tool for investigating the properties of metals (and semiconductors), and then give a few examples of possible applications. The coupling of charge and spin enables the use of highly sensitive electronic measurements to probe magnetic interactions. The technique is experimentally convenient; it requires only one good surface, and can be used on very small samples, in particular, on single crystals. Because the signal is inversely proportional to the sample volume, and because we utilize photolithographic processing with a spatial resolution of order 1 μ, the technique is ideal for the investigation of small systems. Finally, it is a zero frequency, zero field technique, and it is applicable to any material with suitable carrier mobilities and relaxation times. Semiconductors whose carriers have adequate mean free paths will be included in this class of materials if there exist suitable methods for forming ohmic contacts.

In many metals, $g=g(\mathbf{k})=\bar{g}+\delta g(\mathbf{k})$. Here $\delta g(\mathbf{k})$ represents a g anisotropy. Most TESR is performed at 3.2 kG, where the resonance condition is $\hbar\omega_{\mathrm{res}}=g(\mathbf{k})\beta B$. In a single relaxation time, an electron will sample many portions of the Fermi surface, and there will be considerable spread in the g value. In kilogauss fields, the spread in g means that different electrons will resonate at different frequencies, and the resonance is widened so much that relaxation times cannot be measured (the resonance is unobservable). In zero field there is no contribution from these g anisotropies, and relaxation processes can now be studied in these metals. Also, standard TESR requires a thin, foil or film sample, and it is difficult to examine single crystals. Our experimental geometry requires only small samples, and is therefore well suited to this endeavor.

Many other systems have properties of interest that are altered or destroyed in kilogauss fields. Most superconductors have critical fields of a few hundred (or up to a couple of thousand) gauss. Vier and Schultz[18] observed TESR in a type-II superconductor (niobium) just below $H_{c,2}$, and this is the only observation of TESR in a bulk superconductor. With the new method, one could inject and detect spins at fields that span $H_{c,1}$, to investigate the quasiparticle density of states and the nature of flux vor-

tices. Spin glasses and Kondo systems are two other examples of systems that are altered by magnetic fields. The existing probes of conduction-electron dynamics (Mössbauer effect, NMR, ESR) are not able to study the dynamics in small fields,[19] near the spin-glass freezing temperature, which is precisely the range of greatest interest. Spin injection would be well suited to this.

The geometry is convenient for studying surfaces. By cutting a small slot in the sapphire substrate, the back surface of the sample could be readily available to alteration *in situ*. One could adsorb rare gases,[20] or evaporate other materials (noble metals or even ferromagnetic or antiferromagnetic materials) in a controlled fashion to study the spin-orbit interaction with the modified surface.

Because the signal is inversely proportional to the sample volume, the technique is ideal for studying small systems. For example, our sample volume is currently $\approx 10^{-6}$ cc. From Eq. (5), we calculate that the total number of spins that we are detecting is $\Delta N = 10^6$. It would be technically achievable, using molecular beam epitaxy and more sophisticated photolithography, to make our samples 100 times smaller in each dimension. Then $\Delta N = 1$, and one could look for finite-size and single spin effects (one might ask, for example, whether the sample had an even or an odd number of electrons). On a reduced scale, the increased linewidth may make the Hanle effect impractical for measuring relaxation. However, one could lay down a grid of detecting probes at regular intervals from the injector, and measure δ_s directly.

Another novel application would be to look for quantum fluctuations in magnetic conductance (interference in the spin degree of freedom portion of the wave function for spin polarization currents). Finally, we note that there are obvious applications to studying interfaces, the band structure near E_F of ferromagnets, and materials with very short relaxation times (such as heavy fermions, ferromagnets).

We have presented details of an experiment which verifies the idea that a coupling between charge and spin exists at the interface between a ferromagnetic and a paramagnetic metal. The qualitative predictions of the model presented in I are confirmed; quantitative fits to the data show that the model gives a consistent description of the results over a large range of the experimental parameters. This experiment also demonstrates a new technique for measuring conduction-electron spin-relaxation times in the limit of zero applied magnetic field. The times measured using the new technique are in excellent accord with existing results from resonance experiments.

ACKNOWLEDGMENTS

The authors wish to gratefully acknowledge J. Lebens and D. McQueeney for technical assistance, and A. Janossy, H. Hurdequint, P. Monod, and J. Long for useful conversations. This work was principally supported by the National Science Foundation-Materials Research Laboratories program through the Cornell Materials Science Center through Grant No. DMR-8217227; additional help from the Cornell Program on Submicron Structures (PROSUS) and the National Resource and Research Facility for Submicron Structures (NRRFSS) is also acknowledged.

[1]Mark Johnson and R. H. Silsbee, Phys. Rev. B **35**, 4959 (1987).

[2]Commercial SHE Corporation SQUID [now Biotechnology Incorporated (B.T.I.)].

[3]Data have been taken from strictly dc to 24 Hz. There may be applications of the technique in which it will be desirable to work at audio frequencies. For example, one may wish to use a transformer to impedance match the SQUID to a detector junction with relatively large resistance (refer also to Appendix B of I).

[4]R. P. Giffard, R. A. Webb, and J. C. Wheatley, J. Low Temp. Phys. **6**, 533 (1972).

[5]Mark Johnson, Ph.D. dissertation, Cornell University, 1986 (unpublished).

[6]M. Johnson and R. H. Silsbee (unpublished).

[7]Neil W. Ashcroft and N. David Mermin, *Solid State Physics* (Holt, Rinehart, and Winston, New York, 1976), Eq. (2.65). 1976), Eq. (2.65).

[8]*Handbook of Thin Films Technology,* edited by Leon I. Maissel and Reinhard Glang (McGraw-Hill, New York, 1970), Chap. 17.

[9]See, for example, Ref. 17 of I, Eq. (29.30).

[10]L. Finegold, in *Techniques of Metal Research,* edited by R. F. Bashash (Wiley, New York, 1972), Vol. VI, Chap. 3, part 1.

[11]We later initiated the practice of calibrating each data group with the bridge.

[12]R. H. Silsbee and Francois Beuneu, Phys. Rev. B **27**, 2682 (1983).

[13]D. Lubzens and S. Schultz, Phys. Rev. Lett. **36**, 1104 (1976).

[14]See Ref. 4 of I.

[15]We have always assumed, on the basis of ESR bimetal experimental results, that spin-flip scattering at the interface is negligible. If this were *not* the case, the observed η would be diminished as a result.

[16]N. F. Mott, Proc. R. Soc. London, Ser. A **153**, 699 (1936).

[17]N. F. Mott and H. Jones, *The Theory of the Properties of Metals and Alloys* (Clarendon, Oxford, 1936).

[18]D. V. Vier and S. Schultz, Phys. Lett. **98A**, 283 (1983).

[19]See, for example, K. Binder and A. P. Young, Rev. Mod. Phys. **58**, 801 (1986).

[20]D. M. Eigler and S. Schultz, Phys. Rev. Lett. **54**, 1185 (1985).

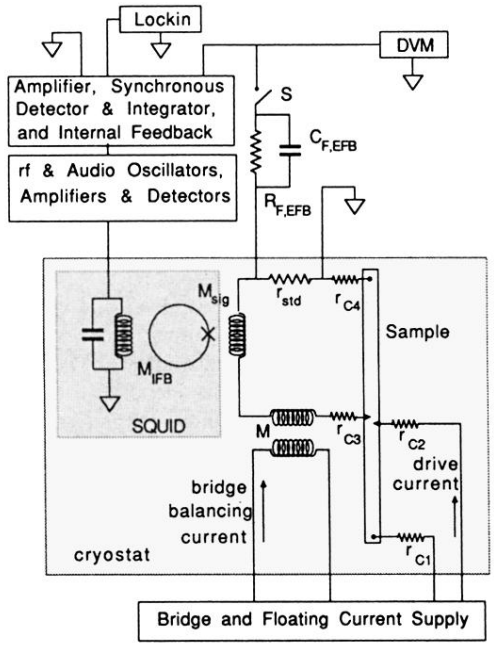

FIG. 1. Schematic diagram of the detector circuit, including the SQUID, the feedback electronics, and the bridge.

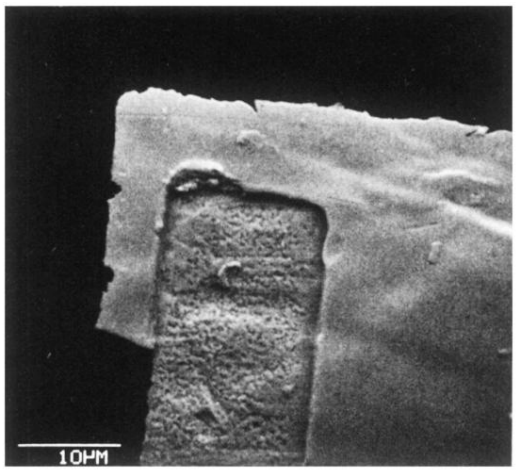

FIG. 4. SEM of window and pad from the control sample, Walrus 8. The light area is a 2600 Å gold film, the dark is polyimide with*out* metalization over the bulk aluminum bar sample. The window has been etched through the polyimide to the surface of the aluminum. Note that the surface is pitted. The film of the pad lies on top of the insulating polyimide, which is a micron thick. Note that the film of the pad has a smooth surface. The film is continuous and overlaps the window, making interfacial contact with the aluminum over the area of the window. At lower left, part of the pad has been torn off during "liftoff."